NeuroImage: Clinical 12 (2016) 858–868

Contents lists available at ScienceDirect

NeuroImage: Clinical

journal homepage: www.elsevier.com/locate/ynicl

Delineation of cortical pathology in multiple sclerosis using multi-surface magnetization transfer ratio imaging

David A. Rudko[a,b,*], Mishkin Derakhshan[a], Josefina Maranzano[a,b], Kunio Nakamura[c], Douglas L. Arnold[a,b], Sridar Narayanan[a,b]

[a] McConnell Brain Imaging Centre, Montreal Neurological Institute and Hospital, McGill University, Montreal, Quebec, Canada
[b] Department of Neurology and Neurosurgery, McGill University, Montreal, Quebec, Canada
[c] Department of Biomedical Engineering, Lerner Research Institute, Cleveland Clinic, 9500 Euclid Avenue Cleveland, OH 44195, United States

ARTICLE INFO

Article history:
Received 24 June 2016
Received in revised form 23 September 2016
Accepted 11 October 2016
Available online 13 October 2016

Keywords:
Multiple sclerosis
Sub-pial demyelination
Cortical surface
Magnetization transfer ratio
MRI

ABSTRACT

The purpose of our study was to evaluate the utility of measurements of cortical surface magnetization transfer ratio (csMTR) on the inner, mid and outer cortical boundaries as clinically accessible biomarkers of cortical gray matter pathology in multiple sclerosis (MS). Twenty-five MS patients and 12 matched controls were recruited from the MS Clinic of the Montreal Neurological Institute. Anatomical and magnetization transfer ratio (MTR) images were acquired using 3 Tesla MRI at baseline and two-year time-points. MTR maps were smoothed along meshes representing the inner, mid and outer neocortical boundaries. To evaluate csMTR reductions suggestive of sub-pial demyelination in MS patients, a mixed model analysis was carried out at both the individual vertex level and in anatomically parcellated brain regions. Our results demonstrate that focal areas of csMTR reduction are most prevalent along the outer cortical surface in the superior temporal and posterior cingulate cortices, as well as in the cuneus and precentral gyrus. Additionally, age regression analysis identified that reductions of csMTR in MS patients increase with age but appear to hit a plateau in the outer caudal anterior cingulate, as well as in the precentral and postcentral cortex. After correction for the naturally occurring gradient in cortical MTR, the difference in csMTR between the inner and outer cortex in focal areas in the brains of MS patients correlated with clinical disability. Overall, our findings support multi-surface analysis of csMTR as a sensitive marker of cortical sub-pial abnormality indicative of demyelination in MS patients.

1. Introduction

It is now widely recognized that standard MR imaging of multiple sclerosis (MS) can visualize only a fraction of the disease burden in cortical gray matter (cGM). In particular, conventional MRI applied at the clinically accessible MRI field strengths of 1.5 or 3 Tesla (T) cannot adequately detect the cortical gray matter pathology observed in postmortem studies, even though cGM pathology is believed to play a significant role in both cognitive dysfunction (Nielsen et al., 2013; Papadopoulou et al., 2013) and worsening clinical symptoms (Cohen-Adad et al., 2011; Nielsen et al., 2013; Mainero et al., 2015). This inability of standard MRI to visualize cortical pathology may partially contribute to the relatively weak association between MRI-visible lesions and clinical status.

A further complicating factor is that the spatial resolution and contrast of standard MRI scans at 1.5 T and 3.0 T are insufficient to detect the important sub-pial demyelination that appears to exist preferentially along the outer layer of the cortex (Peterson et al., 2001). To date, cortical sub-pial demyelination has only been visually observed *in-vivo* using ultra-high field (UHF) MRI at 7 T (Mainero et al., 2009; Cohen-Adad et al., 2011; Nielsen et al., 2012). For example, recent 7 T MRI studies employing T_2^* mapping have demonstrated longer T_2^* values suggestive of demyelination along the layers of the cortex in MS patients (both RRMS and SPMS) compared to controls (Mainero et al., 2015). Regrettably, UHF MRI (≥7 T imaging) is not feasible for large-scale MS clinical trials in the foreseeable future. Currently, there is only one 7 T human MRI system in Canada and approximately 50 worldwide. In contrast, over 2500 3 T systems operate globally. Since multi-center trials required for late stage drug development in MS involve hundreds of clinical sites around the world, 1.5 or 3 T systems remain the only clinically feasible options presently available. The current inability of these systems to efficiently visualize and quantify the extent of cortical pathology remains a major impediment to assessing its response to disease modifying therapies.

In this study, we address these issues using multi-surface, longitudinal measurements of magnetization transfer ratio (MTR) at the clinically-accessible MRI field strength of 3 T. MTR imaging is a semi-

* Corresponding author at: McConnell Brain Imaging Centre, Montreal Neurological Institute, McGill University Institute, 3801 Rue University, Montreal, Quebec, Canada.
E-mail address: david.rudko@mcgill.ca (D.A. Rudko).

http://dx.doi.org/10.1016/j.nicl.2016.10.010

quantitative MRI technique that is sensitive to the relative degree of myelination in brain tissue (Dousset et al., 1992). It has been applied extensively in MS white matter research (Campi et al., 1996; Filippi et al., 1998; Pike et al., 1999; Rocca et al., 1999). More recently, several studies have demonstrated the utility of cortical MTR mapping for tracking demyelination in MS both *in vivo* and in post-mortem tissue samples (Schmierer et al., 2004; Chen et al., 2013; Derakhshan et al., 2014). Our previous work (Derakhshan et al., 2014) at 1.5 T, as well as the work of Samson et al. (2014), suggest subtle cortical demyelination effects can be monitored using MTR projected onto the cortical surface.

The vertex level analysis conducted in our study is supplemented by cortical surface region of interest (ROI) analysis for assessing anatomically-localized regions of the cortex where group-level, age-related decline in csMTR of MS patients exceeds that of controls. A number of previous studies have shown that age-related decline in MTR occurs in the white matter of healthy subjects (Silver et al., 1997; Schiavone et al., 2009; Newbould et al., 2014). One study identified a quadratic decrease in MTR in selected regions of cortical gray matter that occurs predominantly after 40 years of age in healthy control subjects (Mascalchi et al., 2014). To date, however, no link between sub-pial demyelination and subject age of MS patients has been found.

We test the hypothesis that the relative difference in csMTR existing between cortical surface layers in patients correlates with clinical disability in MS, as measured by the Expanded Disability Status Scale (EDSS) (Kurtzke, 1983). Lastly, we compare csMTR values in manually segmented cortical lesions to normal-appearing gray matter (NAGM).

2. Materials and methods

2.1. Study design

Twenty-five patients with MS and 12 age and sex-matched controls were recruited from the Multiple Sclerosis Clinic of the Montreal Neurological Institute and Hospital between November 2009 and November 2010. Subject recruitment was part of a larger ongoing, longitudinal study of cortical demyelination in MS. To this end, 18 patients and 10 controls were imaged at baseline, as well as at a two-year time point to evaluate longitudinal changes in cortical MTR. Overall, the total number of examinations included in our analysis was 65.

Patient inclusion criteria were as follows: (i) subjects must have been between the ages of 20 and 70 and (ii) must have had a diagnosis of MS according to the 2005 McDonald criteria (Polman et al., 2005). Patients were not scanned within two months of a clinical relapse. All patients were on a stable treatment regime (*i.e.* they were not in the process of changing treatment and had no immediate plans to start or change treatment). There were no restrictions on the type of disease-modifying therapies used by the patients enrolled in the study. Of the 25 patient data sets analyzed, 21 had a diagnosis of relapsing-remitting MS (RRMS), while four had a diagnosis of secondary progressive MS (SPMS). The mean age of patients at baseline was 48, with ages ranging from 28 to 67. All MS patients enrolled in the study were clinically evaluated within three months of their scan date by a senior neurologist at the Multiple Sclerosis Clinic of the Montreal Neurological Institute and Hospital. At the time of evaluation, the EDSS score of each patient was determined. Written informed consent was obtained from all patients and controls; the research was approved by the Research Ethics Board of the Montreal Neurological Institute.

2.2. Imaging protocol

Imaging was performed on a 3 T MRI scanner (Siemens Healthcare, Erlangen, Germany) using a volume coil for radiofrequency (RF) excitation and a 12 channel coil for signal reception. Axial T_1-weighted images were acquired using a 3D spoiled gradient-recalled echo sequence with the following scan parameters: TR = 20 ms, TE = 5 ms, flip angle = 27 degrees, field of view = 256 × 192 × 192 mm^3, matrix dimensions = 256 × 192 × 192, isotropic spatial resolution of 1 mm^3 and total scan time = 9 min and 38 s. The T_1-weighted images were used for cortical surface reconstruction, cortical/white matter lesion segmentation and normalized brain volume measurements.

Four additional contrasts, also employed for lesion segmentation, were collected: Axial 2D, T_2-weighted images were acquired using a turbo spin-echo (TSE) sequence with TR = 4500 ms, TE = 83 ms, echo spacing = 9.18 ms, turbo factor = 11, field of view = 256 × 256 × 180 mm^3, matrix dimensions = 256 × 256 × 60, in-plane resolution of 1 mm^2, slice thickness = 3 mm, and total scan time = 3 min and 47 s; Sagittal 3D FLAIR images acquired using an inversion-prepared variable flip angle TSE sequence with TI = 2200 ms, TR = 6 s, TE = 355 ms, echo spacing = 3.3 ms, turbo factor = 141, field of view = 256 × 256 × 176 mm^3, matrix dimensions = 256 × 192 × 176, isotropic 1 mm^3 spatial resolution, GRAPPA acceleration factor R = 2 in the first phase encode direction and total scan time = 8 min and 50 s; Axial 2D, proton density weighted images were acquired using a TSE sequence with TR = 2200 ms, TE = 10 ms, echo spacing = 10.2 ms, turbo factor = 4, field of view = 256 × 256 × 180 mm^3, matrix dimensions = 256 × 192 × 60, in-plane resolution of 1 mm^2, slice thickness = 3 mm, and total scan time = 4 min and 48 s; Sagittal 3D double inversion recovery (DIR) images were acquired with a variable flip angle TSE readout, TI = 3000 ms, TR = 7.5 s, TE = 323 ms, echo spacing = 3.02 ms, turbo factor = 256, field of view = 288 × 243 × 180 mm^3, matrix dimensions = 256 × 192 × 176, isotropic 1.5 mm^3 spatial resolution, GRAPPA acceleration factor R = 2 in the first phase encode direction and total scan time = 6 min and 53 s.

Magnetization transfer ratio (MTR) maps were produced based on (i) an axial gradient echo acquisition with a Gaussian off-resonance saturation pulse +1200 Hz away from the water resonance (Sat) and (ii) a second identical acquisition without the saturation pulse (NoSat). Both the MTR sequences utilized a 3D acquisition with TR = 33 ms, TE = 3.81 ms, flip angle = 10 degrees, field of view = 256 × 192 × 192 mm^3, matrix dimensions = 256 × 192 × 192, isotropic 1 mm^3 spatial resolution, and GRAPPA acceleration factor R = 2 in the first phase encode direction. The acquisition time for each of the MTR sequences was 6 min and 34 s. To calculate MTR maps, both images were registered to the space of the T_1-weighted image using a hierarchical linear registration (Collins et al., 1994). At each voxel, MTR was calculated from the Sat and NoSat image intensities as 100 × (NoSat − Sat) / NoSat.

2.3. Image processing

Cortical surface meshes along the white matter and pial surfaces were first generated based on the T_1-weighted image volumes of each patient at each time point using the standard FreeSurfer analysis pipeline (Dale et al., 1999; Fischl et al., 1999a,b), version 5.1.0. All cortical surface reconstructions were visually inspected, with manual corrections applied if necessary. The FreeSurfer longitudinal analysis pipeline was then used to create unbiased, longitudinally consistent cortical surfaces for the two time points in our study. Based on the resultant white matter and pial surfaces, intermediate surfaces were generated at 25% (outer), 50% (mid) and 75% (inner) depth intervals along a Euclidean distance vector linking a vertex on the pial boundary and the white matter surface (Fig. 1) utilizing in-house developed software. To avoid partial volume contamination from cerebrospinal fluid and white matter that would occur if the pial and white matter boundaries themselves were used, the outer and inner surfaces were defined at depths of 25% and 75% respectively. Note that, in Fig. 1, the green line may not appear halfway between the red and yellow surfaces at all points because we are only looking at a particular 2D slice from a 3D volume.

To evaluate the MTR along each surface, MTR images were registered to the space of the T_1-weighted image and blurred along the surfaces by employing a 2D geodesic smoothing kernel with a full-width at half

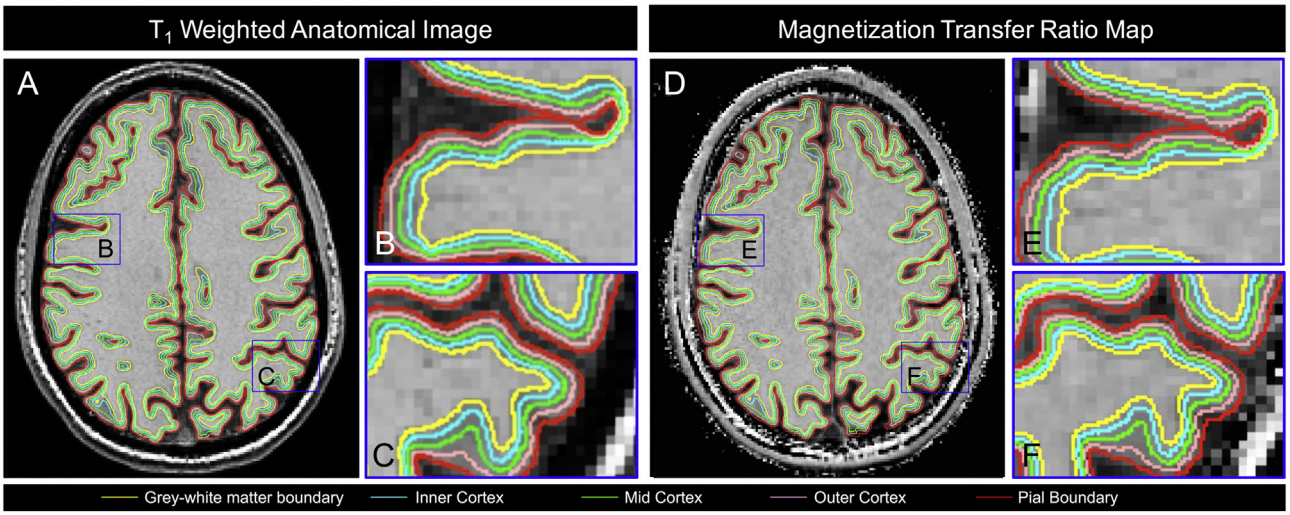

Fig. 1. Representative cortical surface reconstruction examples. Segmentation of the inner (cyan), mid (light green) and outer (pink) cortical surface layers based on the initial FreeSurfer pial and white matter surfaces derived from the longitudinal FreeSurfer pipeline. MR images correspond to one slice from a normal control subject for (A) T_1-weighted anatomical scan and (D) MTR map. Panels B, C, E and F display magnified views of cortical sulci and gyri. The mid cortex (light green) is located along a Laplacian boundary, halfway between the red and yellow surfaces in 3D space. Note that, in the figure, the light green surface layer may not appear to be exactly halfway between the red and yellow surfaces at all points because the figure demonstrates only a 2D slice from a 3D volume.

maximum (FWHM) of 10 mm. Lerch and Evans (2005) have shown that, for quantitative surface-based analysis, 2D geodesic smoothing is preferentially sensitive and reduces partial volume errors and bias compared to conventional 3D isotropic smoothing. Previous research in our lab identified that, at 1.5 T, a geodesic smoothing kernel with a full width at half maximum (FWHM) of 10 mm preferentially detects medium to large areas of sub-pial abnormality suggestive of cortical sub-pial demyelination (Derakhshan et al., 2014). In addition to measuring magnetization transfer ratio along the cortex, FreeSurfer-based cortical thickness measurements were carried out.

The baseline normalized brain volume of each subject was measured using the SIENAX tool from the FSL software package (Jenkinson et al., 2012). White matter MS lesions were automatically segmented employing a Bayesian classifier (Francis, 2005). Following this, a research radiologist having over 10 years experience (J.M.), manually corrected any errors in the white matter lesion masks.

For cortical lesion segmentation, labels were drawn manually in each slice if regions included at least 3 contiguous voxels with hypo-intensity on T_1-weighted images and a corresponding hyper-intensity on T_2-weighted, FLAIR and DIR images. All cortical lesions were segmented by a research radiologist having over 10 years of experience (J.M.), using a multi-contrast reading protocol. The cortical lesion masks were then registered to the MTR maps to allow comparison of the mean MTR in cortical lesions to that in the corresponding cortical regions of controls. The white and gray matter masks derived from the Bayesian classifier were used to calculate mean MTR in normal-appearing cortical gray matter (NACGM) and in normal-appearing white matter (NAWM). The mean MTR in these tissues was compared between patients and controls using a Welch's two-sample *t*-test.

2.4. Surface and volume based statistical analyses

To perform statistical analysis at the group level, all cortical surface reconstructions were non-linearly registered to the coordinate space of the FreeSurfer average template (Dale et al., 1999). Subsequently, vertex-wise statistical analysis of MTR differences between MS patients and controls was carried out using a general linear mixed-effects model. The mixed-effects model included fixed effects terms for both age and group (either MS or controls), as well as a random subject-specific effects term that induced equal correlations between observations of the same subject. Since the mixed effects model was evaluated at each individual vertex, correction for multiple comparisons was carried out to yield accurate statistical results. In our study, this was performed using the resampling-based false discovery rate strategy introduced by Yekutieli and Benjamini (1999), Benjamini and Yekutieli (2001). False discovery rate (FDR) correction was performed using a q-value threshold of 0.1. Such a q-threshold defines the fraction of false positives tolerable in statistical analyses. The mixed effects model was used because measurements of MTR at baseline and two-year time points were strongly correlated. Not all subjects imaged at baseline were able to return for a follow-up scan, leading to missing data. Specifically, 18 out of the total 25 MS patients and 10 out of 12 controls returned for scans at the second time point. The mixed-effects model, with a random subject effect, accounted for missing data at the follow-up scan. The aforementioned statistical analysis was applied for all three cortical surface layers (inner, mid and outer – defined as cyan, light green and pink in Fig. 1).

To augment the above analyses, we tested the hypothesis that MS patients exhibit a significantly greater reduction in csMTR on the outer surface compared to the inner surface, when accounting for the natural gradient of MTR values in controls. Specifically, the average csMTR at each vertex of the controls was subtracted from the surfaces of each MS patient. The result was then normalized by the mean csMTR in controls and used as input to a general linear mixed model. This procedure increased the number of degrees of freedom ($df = 130$) compared to the tests between patients and controls on a single surface ($df = 62$). As a result, additional explanatory variables were able to be included in the mixed-effects model for between-surface analysis. Specifically, the resultant model included fixed effects for age, EDSS, white matter lesion load and normalized brain volume at baseline, as well as a random subject-specific effect.

In addition to the vertex-wise analysis discussed above, we applied ROI-level analyses to investigate: (i) group-level, age-related decline in csMTR of MS patients relative to controls and (ii) age-adjusted, group mean differences in csMTR between MS patients and controls. For this purpose, surface-based ROIs from the Desikan-Killiany atlas (Desikan et al., 2006) were employed. Calculating mean surface csMTR within these ROIs increases the effective SNR relative to vertex-based analyses. We hypothesized this would allow better detection of age-related reductions of csMTR. For each ROI, a mixed model analysis with fixed effects terms for age and group (either MS or controls), as well as a random subject-specific effect was carried out. The mixed model analysis was conducted independently for the left hemisphere,

the right hemisphere and both hemispheres combined. For the combined hemispheres, an additional fixed effect specifying the hemisphere for each subject was included. Multiple comparisons correction of the ROI data was performed using FDR with a q threshold of 0.05.

3. Results

3.1. Subject demographic and clinical information

The mean age of patients in our study was 48.5 ± 9.5 and the mean age of controls was 42.1 ± 11.8. The control group consisted of 12 subjects imaged at baseline and 10 subjects at the second year time point. The MS patient group consisted of 25 subjects at baseline and 18 subjects at the second year time point. Additional demographic details, including gender, median baseline white matter lesion load and EDSS are presented in Table 1.

3.2. Whole-brain MTR

Our first analysis examined the mean csMTR across the entire cerebrum. This was used to discern differences in cerebral cortical myelination patterns between MS patients and controls. Only the baseline time point data was used for this analysis. Examples of baseline time point csMTR along the inner, mid and outer cortical boundaries for MS patients and controls are displayed in Fig. 2A. The natural gradient in cortical myelination is appreciable, based on the decreasing MTR values (darker green colours) seen when moving from the inner to the outer cortical boundaries. The mean cerebral csMTR of MS patients compared to controls is summarized in the bar plots of Fig. 2B. Mean csMTR of patients was significantly reduced ($p < 0.05$) on the mid and outer cortices. The expected natural gradient in csMTR from inner to outer cortex was also observed in these plots - decreasing from the inner to the outer boundary. The csMTR of controls decreased by 2.78 MTR units from the inner to the outer surface, while the csMTR of patients decreased by 3.52 units The absolute differences between the inner cortex and the mid cortex (0.55 MTR units for controls, 1.36 units for patients) were significantly ($p < 0.05$) smaller than those between the mid cortex and the outer cortex (2.23 units for controls, 2.16 units for patients).

3.3. Surface-based MTR at the vertex level on individual surfaces

Localized reductions in csMTR of patients compared to controls along the inner, mid and outer cortical surface boundaries are identified with colour overlays in Fig. 3. Regions of significant csMTR reduction in MS patients compared to controls are indicated by the blue colours in the thresholded t-statistic maps (Fig. 3B). The vertex-wise analysis shown in Fig. 3 used a general mixed model analysis with a fixed age covariate and a random subject covariate. The largest areas of sub-pial MTR abnormality were identified along the outer cortical boundary. The percentage of affected cortical surface area, as defined by our false discovery rate multiple comparisons correction, decreased from 27.18% along the outer surface to 7.24% along the inner surface (Fig. 3). The largest areas of reduced csMTR on the outer cortical boundary extended along the superior temporal, parahippocampal, superior/inferior parietal and posterior cingulate cortices, as well as in the precuneus, cuneus and precentral gyrus of both hemispheres. Translaminar differences in csMTR (those regions which were significant on all cortical surface layers) were also identified across cortical regions in the left parahippocampal and inferior parietal cortices, as well as in the right posterior cingulate cortex.

3.4. Brain parcellation approach for evaluating age-related changes in csMTR

The relationship between layer-specific csMTR and patient age in three selected brain ROIs (precentral cortex, posterior cingulate cortex and precuneus), parcellated using the Desikan-Killiany FreeSurfer atlas (Desikan et al., 2006), is displayed in Fig. 4A–C. These three ROIs were chosen because of their anatomical and functional roles in large-scale brain networks and also because of the patterns we observed in either (i) significantly reduced group-average csMTR or (ii) significant age-related reductions in csMTR of patients compared to controls. Age was used as an independent variable in the mixed model regression of Fig. 4. This allowed csMTR of both patients and controls to be easily visualized on the same graph. All correlation coefficients and p-values presented in Fig. 4A–C were derived from mixed-model analysis at the ROI level. The blue (precentral cortex), red (posterior cingulate) and orange (precuneus) data points represent individual subjects at either baseline or two-year time points. For clarity, baseline and two-year time points for each individual patient are connected by dotted lines. The bold dotted lines in Fig. 4A–C identify the linear regression model fit, the solid black lines represent the change in csMTR of controls as a function of age and the light gray shaded area indicates the 95% confidence intervals of each fit. The corresponding regression slopes and p-values in all other parcellated brain regions showing either (i) significantly reduced mean csMTR or (ii) significant age-related reductions in csMTR of patients compared to controls are displayed in Table 2.

In Fig. 4B, in the outer layer of the posterior cingulate cortex, a significant age-related reduction in csMTR was observed in MS patients compared to controls ($p < 0.05$ and significant after multiple comparisons correction using the false discovery rate technique with a threshold of $q = 0.1$). In the middle layer of the posterior cingulate cortex, a trend towards significant age-related csMTR reduction was observed ($p < 0.05$, but not found to be significant after multiple comparisons correction with $q = 0.1$). Age-related reduction in csMTR along the inner layer of the posterior cingulate cortex was not significant and no trend was observed. In the outer cortical layer of the precuneus, a trend was noted in the age-related reduction of csMTR ($p = 0.014$, but not significant after multiple comparisons correction). Age-related reductions in csMTR were not observed along the middle or inner layers.

Inside the cortical ROIs that showed either statistically significant age-related decreases in csMTR or trends in csMTR decrease, there was an average 0.092 MTR units/yr decrease on the outer surface. In contrast, in corresponding ROIs along the mid and inner cortex, the average annual decreases were 0.039 MTR units/yr and 0.046 MTR units/yr respectively.

Table 1
Demographic and clinical data.
Demographic and clinical data for our study cohort (all data showing error estimates represent mean ± standard deviation). EDSS refers to the Expanded Disability Status Scale.

Variable	Controls	Patients
Number of participants	12 at baseline time point, 10 at second year time point	25 at baseline time point, 18 at second year time point
Sex (M/F)	4/8 at baseline time point, 4/6 at second year time point	7/18 at baseline time point, 5/13 at second year time point
Baseline age, mean (range)	42.10 (22–60)	48.48 (28–67)
Baseline EDSS, mean (range)	Not applicable	2.92 (0–8)
Baseline normalized brain volume (mL), mean ± std. dev.	1473.10 ± 91.22	1452.70 ± 95.01
Baseline white matter lesion load (mL), median (range)	Not applicable	34.8 (8.7–48.0)

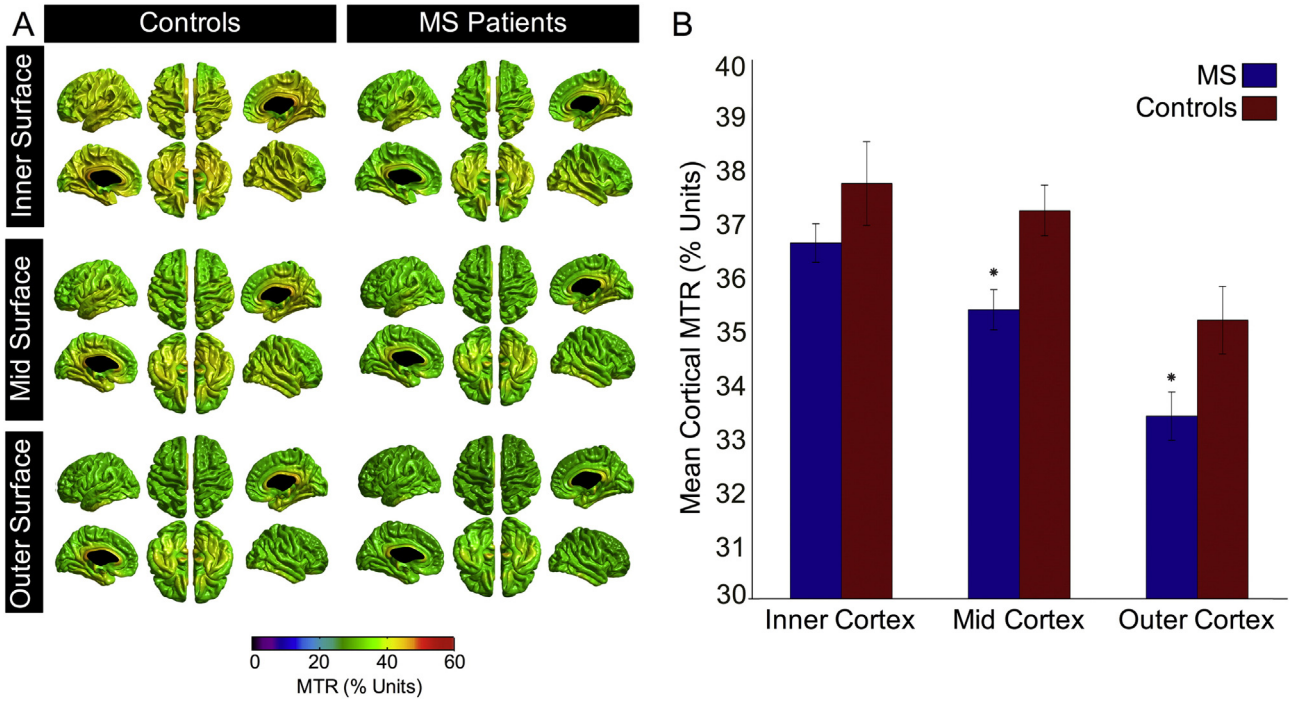

Fig. 2. Cortical surface MTR maps at three cortical depths. (A) Representative csMTR smoothed along the inner, mid and outer cortical boundaries for controls (left column) and MS patients (right column). The MTR values are windowed between 0 and 60 MTR units. (B) Mean MTR across the inner, mid and outer surfaces for the whole brain. Error bars represent standard deviations (*represents $p < 0.05$). The inter-hemispheric cut has been masked-out (blacked-out regions) to remove spurious MTR values from this region.

The columns labeled "main effect" in Table 2 identify in bold all the ROIs where csMTR of patients was lower, on average, compared to controls. Specifically, in the pars opecularis, rostral anterior cingulate, rostral middle frontal and lateral orbitofrontal cortices, the average csMTR was significantly reduced only along the outer surface. Likewise, in the caudal anterior cingulate, precentral and postcentral cortices, only the outer and middle cortical bands showed significantly reduced csMTR.

Cerebral mean MTR in normal-appearing cortical gray matter (NACGM), cortical gray matter lesions and normal-appearing white matter (NAWM) are compared in Table 3. The mean NACGM MTR did not differ between patients and controls, while the NAWM in MS patients was significantly reduced compared to healthy controls at the level $p < 0.05$. The mean cortical gray matter lesion MTR, 34.57 ± 2.60, was significantly reduced ($p < 0.05$) compared to the MTR in the corresponding matched locations in controls (36.39 ± 0.97). For leukocortical lesions, only the portion of the lesion existing within the cortical gray matter was used to calculate the mean MTR values. NACGM included all cortical gray matter tissue without a radiologically identified lesion.

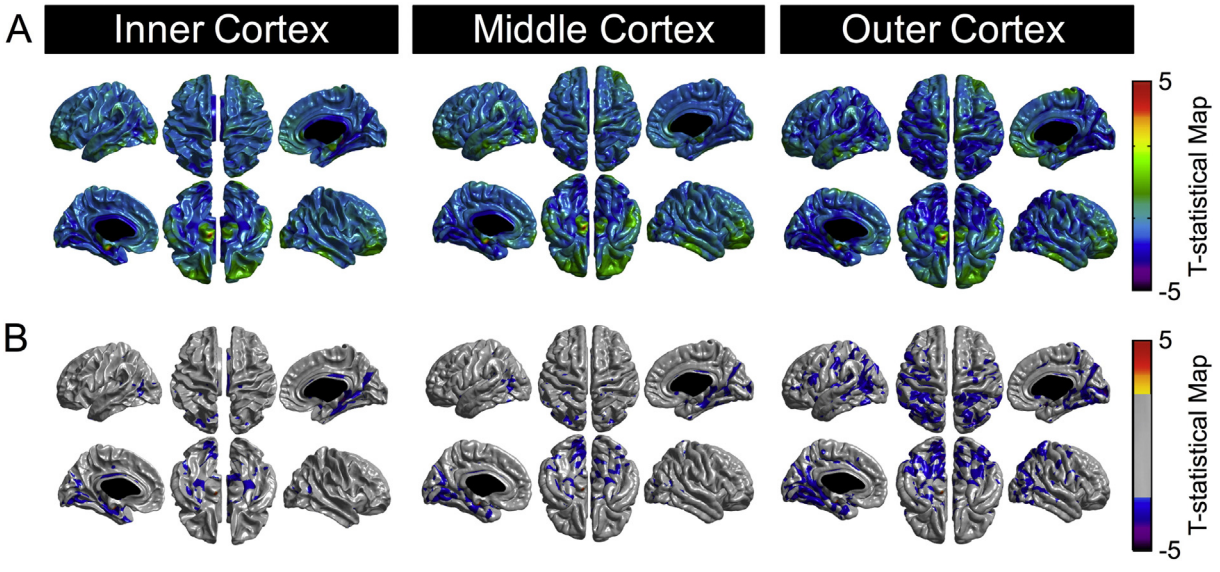

Fig. 3. Vertex-wise t-statistical map comparison between MS patients and controls. Fig. 3A shows group registered, t-statistical maps for inner, mid and outer cortical surfaces displaying regions of significant MTR decrease in patients compared to controls. The maps in Fig. 3B have been multiple comparisons-corrected using the false discovery rate (FDR) technique with $q = 0.05$. Consequently, the corresponding colour bar in Fig. 3B has been thresholded to only show the relevant t-statistical values above the FDR threshold. The inter-hemispheric cut has been masked-out (blacked-out regions) to remove spurious MTR values from this region.

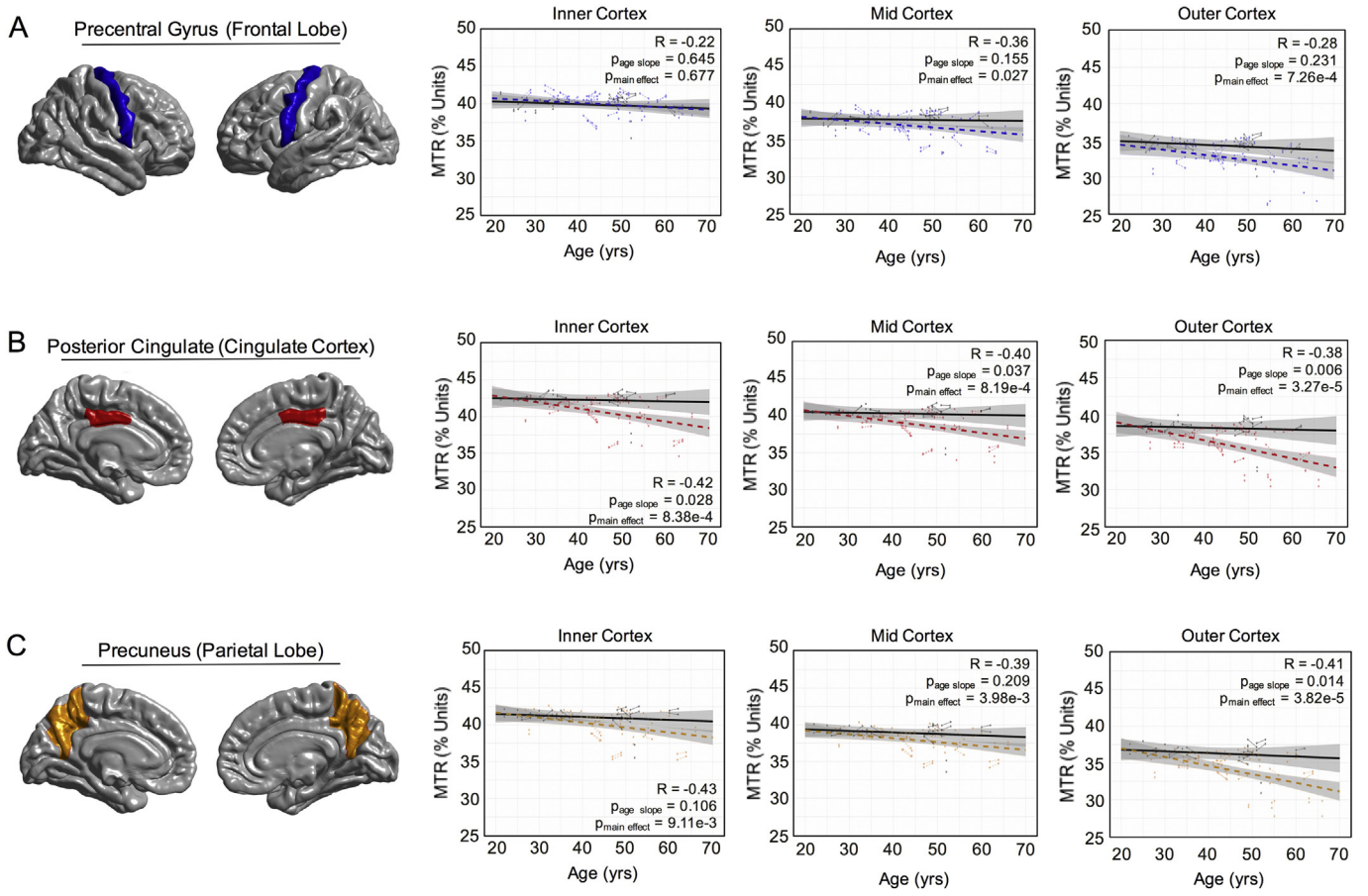

Fig. 4. Age-related decreases in cortical surface MTR in the precentral cortex, posterior cingulate and precuneus. Regional cortical surface MTR decrease as a function of age in our subject cohort. Results are displayed for the three selected ROIs in (A) the precentral cortex (frontal lobe), (B) posterior cingulate (cingulate cortex) and (C) precuneus (parietal lobe). The blue (precentral cortex), red (posterior cingulate) and orange (precuneus) data points represent individual subjects at either baseline or two-year time points. For clarity, baseline and two-year time points for each individual patient are connected by dotted lines. The bold dotted lines in Fig. 4A–C identify the linear regression model fit; the solid black lines represent the change in csMTR of controls as a function of age and the light gray shaded area indicates the 95% confidence intervals of each fit. Correlation coefficients were derived from mixed-model analysis at the ROI level. The p-values displayed on each plot are derived from a mixed model analysis, with fixed effects terms for age, group (either MS or controls) and hemisphere, as well as a random subject-specific effect.

3.5. Surface-based MTR at vertex level using the difference in MTR between surfaces

Using a vertex-wise analysis, we also explicitly examined the relative differences in csMTR between the three cortical surfaces. When all csMTR values were corrected for the natural gradient in csMTR that existed in controls, only the difference between the outer and inner csMTR proved significant (using FDR multiple comparisons correction with $q = 0.05$). This result is shown in Fig. 5. Significant light blue clusters in the thresholded t-statistic maps of Fig. 5 identify regions where the relative decrease in csMTR along the inner surface exceeded that on the outer surface. Clustered, light blue regions exist in the left superior frontal cortex and pars opecularis, as well as in the right superior frontal cortex. The relative decrease in csMTR was greater along the outer cortex (orange/yellow clusters) in the left supramarginal and inferior parietal cortices, as well as in the left and right superior and middle temporal lobes.

Fig. 6 shows thresholded t-statistical maps of regions where the relative csMTR difference between outer and inner cortical MTR of MS patients (corrected for the natural patterns of MTR in controls) was correlated with EDSS. Values are significant after multiple comparisons correction with $q = 0.05$ and after co-varying for normalized brain volume, white matter lesion load, global cortical thickness, global cortical MTR and age. The strongest associations with EDSS were identified in large clusters located in the (A) precuneus, (B,C) superior frontal and (D) rostral anterior cingulate cortices (red squares). Significant t-values were also observed in the vicinity of the primary motor strip, as well as in the left superior frontal, supramarginal, lateral orbitofrontal cortices.

4. Discussion

Cortical pathology may be a substrate of cognitive impairment (Nelson et al., 2011; Nielsen et al., 2013; Papadopoulou et al., 2013) and worsening clinical symptoms in patients with MS (Cohen-Adad et al., 2011; Nielsen et al., 2013). Indeed, areas of sub-pial abnormality suggestive of diffuse sub-pial demyelination have been measured by increases in quantitative T_2^* and T_2^*-weighted signal intensity obtained with UHF 7 T MRI. Such sub-pial abnormalities have previously been linked to increased neurological disability based on both EDSS and the Multiple Sclerosis Severity Score (MSSS) (Nielsen et al., 2013; Mainero et al., 2015). However, UHF MRI will likely not be available for large-scale MS clinical trials in the near future. Moreover, even with gradient echo-based T_2^* mapping at 7 T, the current scan times required for performing sub-millimeter imaging of *whole-cerebrum* cortical laminae with good signal-to-noise ratio and limited artifacts are on the order of 30–45 min (Mainero et al., 2009; Nielsen et al., 2013; Mainero et al., 2015).

Clearly, there is a need for fast, efficient quantitative MRI methods to track cortical pathology in MS clinical studies at accessible field strengths. Cortical MTR has previously been suggested as a quantitative marker of sub-pial demyelination in MS (Crespy et al., 2011; Chen et al., 2013; Derakhshan et al., 2014; Samson et al., 2014). Accordingly, in this

Table 2
Mixed-model analysis of csMTR reductions. A mixed model with age, random subject, and age × group covariate terms was employed. In the case of the hemisphere-combined data, a fixed effect for hemisphere and an interaction between hemisphere and subject index was also included. The columns entitled 'Age, MTR unit/yr' identify both the magnitude of age-related decline of csMTR in MS patients and whether this decline was significant relative to control subjects. The bold font indicates significant values after correction for multiple comparisons. Italic font indicates trends.

Region	Left hemisphere		Right hemisphere		Combined hemispheres	
	Main effect	Age, MTR unit/yr (pval)	Main effect	Age, MTR unit/yr (pval)	Main effect	Age, MTR unit/yr (pval)
Pars opecularis (inner)	0.404	−0.0464 (0.315)	0.938	−0.0434 (0.268)	0.452	−0.057 (0.062)
Pars opecularis (mid)	0.409	−0.0264 (0.493)	0.866	−0.0311 (0.329)	0.454	−0.031 (0.210)
Pars opecularis (outer)	**0.0172**	−0.0564 (0.304)	**0.0147**	−0.0777 (0.169)	**4.80e-4**	−0.071 (0.068)
Posterior cingulate (inner)	**0.0152**	−0.0760 (0.149)	**0.0283**	−0.0800 (0.113)	**8.38e-4**	−0.078 (0.028)
Posterior cingulate (mid)	**0.0187**	−0.0676 (0.171)	**0.0216**	−0.0665 (0.128)	**8.19e-4**	*−0.067 (0.037)*
Posterior cingulate (outer)	**0.0021**	−0.1164 (0.0396)	**0.0076**	−0.1027 (0.070)	**3.27e-5**	**−0.109 (0.006)**
Precuneus (inner)	0.0765	−0.0271 (0.528)	0.0672	−0.060 (0.159)	**9.11e-3**	−0.0481 (0.106)
Precuneus (mid)	0.0535	−0.021 (0.569)	0.0407	−0.038 (0.301)	**3.98e-3**	−0.032 (0.209)
Precuneus (outer)	**5.67e-3**	−0.0834 (0.133)	**3.25e-3**	−0.101 (0.061)	**3.82e-5**	*−0.094 (0.014)*
Rostral ant. cingulate (inner)	0.319	−0.0033 (0.952)	0.744	−0.0466 (0.269)	0.311	−0.023 (0.492)
Rostral ant. cingulate (mid)	0.445	−0.0075 (0.870)	0.814	−0.0463 (0.210)	0.445	−0.030 (0.307)
Rostral ant. cingulate (out)	0.137	−0.065 (0.287)	0.112	−0.0836 (0.146)	**0.025**	*−0.083 (0.047)*
Rostral Middle frontal (inner)	0.459	−0.0121 (0.772)	0.364	−0.00795 (0.850)	0.22	−0.015 (0.605)
Rostral middle frontal (mid)	0.216	−0.0586 (0.148)	0.472	−0.00805 (0.818)	0.65	−0.032 (0.235)
Rostral middle frontal (outer)	**0.0314**	−0.00894 (0.798)	0.335	−0.0353 (0.479)	**0.04**	−0.025 (0.402)
Supramarginal (inner)	**0.0489**	−0.013 (0.798)	0.114	−0.019 (0.701)	**0.011**	−0.019 (0.584)
Supramarginal (mid)	0.0537	−0.007 (0.868)	0.181	−0.021 (0.571)	**0.017**	−0.015 (0.568)
Supramarginal (outer)	**3.53e-3**	−0.084 (0.127)	**6.62e-3**	−0.067 (0.222)	**4.74e-4**	*−0.076 (0.046)*
Caudal ant. cingulate (inner)	0.205	−0.0166 (0.761)	0.147	−0.0532 (0.403)	0.048	−0.038 (0.361)
Caudal ant. cingulate (mid)	0.0846	−0.0509 (0.333)	0.0846	−0.0509 (0.333)	**1.54e-3**	**−0.003 (0.002)**
Caudal ant. cingulate (outer)	**2.34e-3**	−0.0732 (0.1889)	**0.0339**	−0.0618 (0.266)	**1.86e-4**	−0.067 (0.083)
Precentral (inner)	0.860	−0.0181 (0.661)	0.362	−0.0102 (0.826)	0.677	−0.0116 (0.645)
Precentral (mid)	0.0685	−0.0534 (0.228)	0.219	−0.0297 (0.468)	**0.0268**	−0.0420 (0.155)
Precentral (outer)	**0.015**	−0.0122 (0.791)	**0.018**	−0.0766 (0.195)	**7.26e-4**	−0.0446 (0.231)
Paracentral (inner)	0.077	−0.0229 (0.665)	0.030	−0.0356 (0.412)	**5.24e-3**	−0.0328 (0.326)
Paracentral (mid)	0.080	−0.0206 (0.659)	0.102	−0.0398 (0.329)	**1.50e-2**	−0.0334 (0.271)
Paracentral (outer)	**0.013**	−0.0856 (0.225)	**0.017**	−0.112 (0.114)	**4.49e-4**	*−0.1018 (0.038)*
Postcentral (inner)	0.229	−0.0372 (0.409)	0.579	−0.0634 (0.130)	0.1975	−0.0544 (0.0714)
Postcentral (mid)	0.0508	−0.0250 (0.518)	**2.78e-2**	−0.0413 (0.221)	**2.82 e-3**	−0.0339 (0.176)
Postcentral (outer)	**9.49e-3**	−0.0162 (0.753)	**5.36e-3**	−0.0561 (0.269)	**1.12e-4**	−0.0208 (0.558)
Entorhinal (inner)	**5.05e-3**	−0.0323 (0.581)	**3.63e-3**	−0.112 (0.0656)	**3.31e-5**	*−0.083 (0.046)*
Entorhinal (mid)	**1.40e-3**	−0.0312 (0.543)	**2.68e-3**	−0.0830 (0.107)	**7.86e-6**	−0.059 (0.098)
Entorhinal (outer)	**5.58e-4**	−0.0676 (0.208)	**3.99e-3**	−0.0596 (0.186)	**5.83e-6**	−0.065 (0.062)
Fusiform (inner)	**6.78e-3**	−0.0890 (0.216)	**3.91e-3**	−0.1538 (0.0223)	**5.95e-5**	**−0.138 (0.005)**
Fusiform (mid)	**4.37e-3**	−0.0641 (0.265)	**2.68e-3**	−0.0830 (0.107)	**1.40e-5**	*−0.098 (0.010)*
Fusiform (outer)	**7.60e-4**	−0.0493 (0.272)	**3.99e-3**	−0.0596 (0.186)	**3.69e-7**	−0.056 (0.051)
Inf. parietal (inner)	0.0704	−0.0143 (0.769)	**0.0373**	−0.0419 (0.340)	**5.19e-3**	−0.022 (0.498)
Inf. parietal (mid)	**8.67e-5**	−0.0099 (0.746)	**0.0136**	−0.0189 (0.567)	**4.17e-6**	−0.019 (0.402)
Inf. parietal (outer)	**7.98e-6**	−0.0564 (0.180)	**9.28e-4**	−0.0220 (0.592)	**1.87e-8**	−0.040 (0.172)
L. orbitofrontal (inner)	0.163	−0.0141 (0.757)	0.467	−0.0398 (0.471)	0.142	−0.013 (0.709)
L. orbitofrontal (mid)	0.392	−0.0052 (0.895)	0.891	−0.0306 (0.473)	0.624	−0.018 (0.525)
L. orbitofrontal (outer)	**0.0131**	−0.0716 (0.147)	0.170	−0.0572 (0.169)	**5.46e-3**	−0.062 (0.053)
M. orbitofrontal (inner)	0.0931	−0.0720 (0.253)	0.129	−0.0703 (0.303)	**0.021**	−0.072 (0.114)
M. orbitofront. (mid)	0.0931	−0.0669 (0.199)	0.139	−0.0481 (0.385)	**0.020**	−0.057 (0.123)
M. orbitofront. (outer)	**0.0170**	−0.0939 (0.098)	**0.0333**	−0.0758 (0.160)	**0.001**	*−0.088 (0.021)*
M. temporal (inner)	**8.74e-3**	−0.1086 (0.0751)	**0.0146**	−0.1054 (0.0663)	**2.56e-4**	**−0.111 (0.007)**
M. temporal (mid)	**4.42e-3**	−0.0888 (0.0524)	**7.83e-3**	−0.0553 (0.179)	**6.98e-5**	*−0.073 (0.015)*
M. temporal (outer)	**1.53e-4**	−0.0263 (0.385)	**5.80e-4**	−0.0308 (0.320)	**1.09e-3**	−0.021 (0.432)

Table 3
Regional differences in MTR (in MTR units ± standard deviation) between patients and controls (*p < 0.05 relative to corresponding cortical lesion ROI locations in matched controls, ◆p < 0.05 relative to control NAWM).

Brain region	Healthy controls	MS patients
Normal-appearing cortical gray matter (NACGM) MTR	36.31 ± 0.74	35.80 ± 1.36
Cortical gray matter lesion MTR regions of interest	36.39 ± 0.97	34.57 ± 2.60*
Normal-appearing white matter (NAWM) MTR	44.33 ± 2.94	41.16 ± 4.08◆

Values in the table represent mean ± standard deviation.

study, we have utilized *cortical surface-based analysis* of MTR data to quantify sub-pial abnormalities suggestive of diffuse sub-pial demyelination using standard 3 T MRI at a voxel resolution of 1 mm^3 isotropic. We have also explored the use of both individual cortical surface layers and the relative difference in csMTR between those layers as metrics of sub-pial demyelination. Additionally, we have quantified the csMTR values in anatomically parcellated ROIs and manually segmented cortical lesions in order to provide context for our separate voxel-wise csMTR measurements of diffuse, sub-pial abnormality.

Our results suggest that csMTR maps, particularly those created using the outer cortical boundary, are capable of identifying a subset

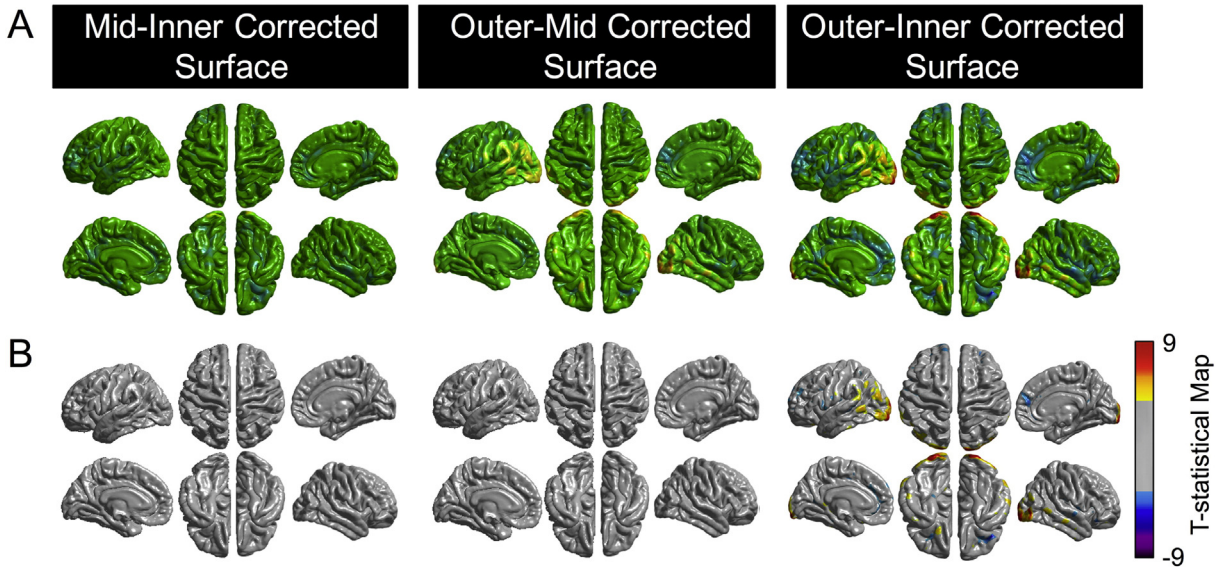

Fig. 5. Vertex-wise statistical maps comparing differences in MTR between cortical surfaces. t-Statistical (Fig. 5A and B) maps displaying between-surface differences in MTR of patients. This analysis was applied to test the hypothesis that MS patients exhibit a significantly greater reduction in csMTR on the outer surface of the cortex compared to the inner surface, when accounting for the natural gradient of MTR values in controls. The average csMTR at each vertex of the controls was subtracted from the surfaces of each MS patient. The result was then normalized by the mean csMTR in controls and used as input to a general linear mixed model with fixed effects for age, EDSS, white matter lesion load, normalized brain volume at baseline, as well as a random subject-specific effect. The maps in Fig. 5B have been multiple comparisons-corrected using the false discovery rate technique with q = 0.05.

of cortical pathology that has been identified in post-mortem immunohistochemistry (Peterson et al., 2001; Bo et al., 2003; Kutzelnigg et al., 2005; Magliozzi et al., 2007; Howell et al., 2011). The finding, presented in Fig. 3, that a larger percentage of outer cortical surface shows decreased csMTR compared to the inner surface (from 27.18% along the outer surface to 7.24% along the inner surface) is in keeping with recent observations by Mainero et al. (2015). Our work supports these recent findings and in addition, extends their scope by utilizing csMTR at multiple cortical levels. In our study, vertex-level csMTR signal reductions were observed along the outer cortical surface in the superior temporal, parahippocampal, superior/inferior parietal, posterior cingulate and inferior parietal cortices, as well as in the precuneus, cuneus and precentral gyrus of both hemispheres. These results are spatially consistent with the patterns of sub-pial demyelination observed in MS patients in post-mortem histopathology studies (Peterson et al., 2001; Bo et al., 2003; Kutzelnigg et al., 2005).

In Fig. 4 and Table 2, we have identified parcellated brain regions that displayed either (i) significantly lower group-average csMTR in patients compared to controls or (ii) significant age-related decreases in csMTR in the cortex of MS patients compared to controls. Statistically significant, age-related reductions in csMTR (and associated trends shown in italics in Table 2) were generally more prevalent along the

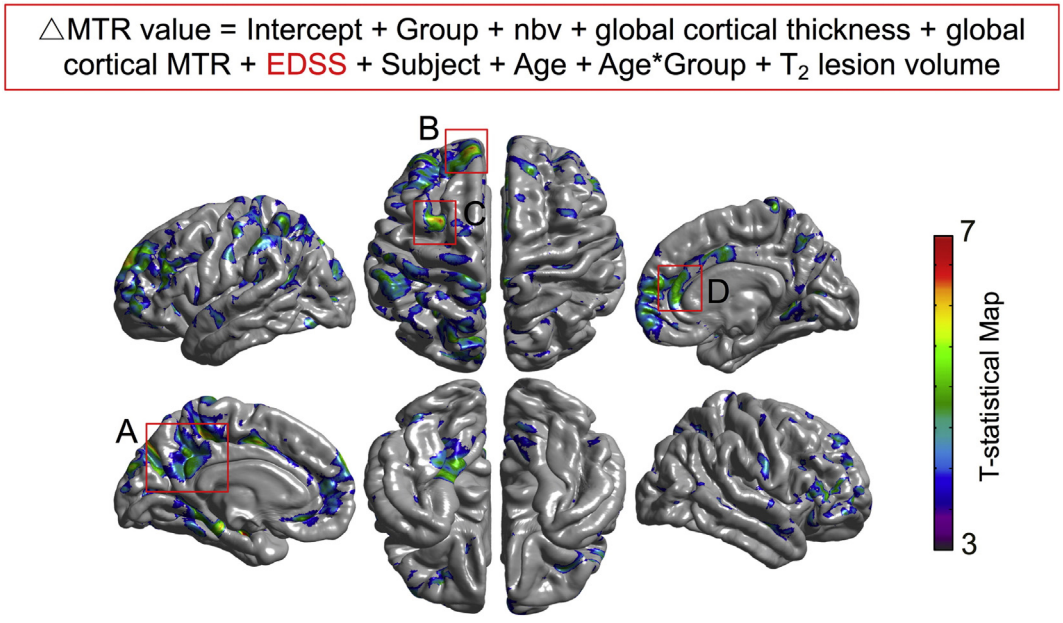

Fig. 6. Thresholded t-statistical maps showing regions where the relative csMTR difference between outer and inner cortical MTR of MS patients (corrected for the natural patterns of MTR in controls) was correlated with EDSS. Values are significant after multiple comparisons correction with q = 0.05. The strongest associations with EDSS were identified in large clusters located in the (A) precuneus, (B,C) superior frontal and (D) rostral anterior cingulate cortices (red squares). As shown in the mixed model equation in the red box at the top of the figure, co-variates for normalized brain volume, white matter lesion load, global cortical thickness, global cortical MTR and age were included in this vertex-wise analysis. nbv = normalized brain volume.

outer and mid cortex compared to the inner cortex. This supports the hypothesis that progressive, age-related sub-pial demyelination in MS may be spatially localized along the outer and mid cortical bands. In particular, the ROIs defining the medial orbitofrontal, rostral anterior cingulate, paracentral, posterior cingulate, supramarginal and precuneus cortices showed trends towards age-related csMTR decrease only along the outer or outer/mid cortex. The rostral anterior cingulate, posterior cingulate and precuneus are involved in executive function, memory and processing speed through thalamo-cortical circuits (Leech and Sharp, 2014). Recent structural and functional MRI studies have identified tissue damage in the thalamo-cortical circuits linked to cognitive impairment and clinical disability in MS (Rocca et al., 2003; Mesaros et al., 2012; Yu et al., 2012; Tona et al., 2014; Tewarie et al., 2015). As a result, age-related csMTR reductions may be biomarkers of progressive loss of cognitive function and accumulation of clinical disability in MS through demyelination of cortical nodes in the thalamo-cortical network.

With reference to the "main effect" columns in Table 2, we identified significant reductions in csMTR compared to controls in the outer caudal anterior cingulate, precentral and postcentral cortices. However, no age-related decline was identified in these regions. A common link between these areas is their high myelin content (Glasser and Van Essen, 2011; Bock et al., 2013; Glasser et al., 2014). This may suggest that, in such regions of naturally occurring high myelin content, either (i) initial demyelination was more severe, so csMTR reached bottom earlier or (ii) repair mechanisms may have allowed cortical pathology to stabilize after an initial period of acute inflammation.

Figs. 5 and 6 illustrate the results of our between-surface, csMTR analysis. For this analysis, csMTR was calculated relative to the mean csMTR on each control surface. The result was then used as input to the longitudinal, linear mixed model with covariates for age, EDSS, white matter lesion load and normalized brain volume at baseline, in addition to a random subject-specific effect which induced equal correlations between observations of the same subject. Two hypotheses were tested: (i) whether the relative csMTR difference between layers was significant (Fig. 5) and (ii) whether there was an association between this difference and EDSS (Fig. 6).

In the group-level maps of Fig. 5, in the superior frontal cortex, pars opecularis, and right superior frontal cortex, the magnitude of the relative decrease in csMTR along the inner surface exceeded that seen on the outer surface (light blue areas in thresholded t-statistic maps). This may be due to inflammatory processes occurring at the gray matter/white matter boundary in these subjects (Geurts et al., 2005; Mainero et al., 2009; Mistry et al., 2014). Indeed, several recent UHF MRI studies have now recognized the prevalence of leukocortical (Type I), T_2^*-hyperintense lesions at the gray matter/white matter boundary (Mainero et al., 2009; Nielsen et al., 2013) and have pointed to their significant association with processing speed as well as learning and memory as measured by neuropsychological testing (Nielsen et al., 2013). Areas where the relative decrease along the outer cortex was larger than that seen on the inner cortex were found in the left supramarginal and inferior parietal cortices, in addition to the left and right superior and middle temporal lobes (orange/yellow areas in thresholded t-statistic maps). These are all highly myelinated regions of the cortex (Glasser and Van Essen, 2011), supporting the notion that highly-myelinated areas may be preferred foci of cortical sub-pial demyelination in MS.

In Fig. 6, we have highlighted regions where the relative difference in csMTR between the outer and inner cortex correlated with EDSS. Highly significant correlations were observed in the left and right rostral anterior cingulate and precuneus, as well as in the left superior frontal cortex. These regions are broadly associated with motor and sensory processing. The rostral anterior cingulate has also been implicated with learning and problem solving (Allman et al., 2001), while the superior frontal gyrus has been related to coordinated action of the sensory processing networks (Goldberg et al., 2006, 2007). The precuneus is subdivided according to its functionality into (i) an anterior sensorimotor area which is connected with the premotor and somatosensory cortices (This could explain the association between reduced outer csMTR and EDSS) and (ii) a cognitive/associative central area linked to both inferior parietal lobule and prefrontal cortical regions (Margulies et al., 2009). The EDSS score itself is weighted towards motor disability which supports the association in our data with reduced outer csMTR in motor networks. EDSS scores have been repeatedly associated with sensorimotor impairments (Zackowski et al., 2009; Zhuang et al., 2015), supporting the sensorimotor network spatial correlations in Fig. 6.

Using high-resolution 7 T data from a multi-echo gradient echo sequence, Mainero et al. recently observed correlations between increased T_2^* (indicative of demyelination) and neurological disability defined by EDSS and MSSS (Mainero et al., 2015). The greatest association was observed on the outer cortical surface for both EDSS and MSSS. However, the reported correlations between surface-based T_2^* and MSSS were very sparse. Further, when using white matter lesion load as a nuisance factor in their vertex-wise general linear model, Mainero et al. found that a number of surface-based correlations with EDSS were removed (Mainero et al., 2015). In our work, white matter lesion load was also used as a nuisance covariate, but it had no effect on the cluster-wise correlations with EDSS (Fig. 6). This may indicate that csMTR is a more stable measure of the cortical pathology that distinctly contributes to neurological disability measured using EDSS.

Mapping of any quantitative MRI parameter (be it MTR, T_2^* or any other metric) on cortical surface layers with a resolution of 1 mm isotropic is inherently challenging due to the thickness of the human cerebral cortex (varying between 1 and 4.5 mm). As shown in Fig. 1, the multilayer cortical surface reconstruction in our study is robust in most regions having thicknesses >3 mm. For regions with thickness <3 mm, the smoothed values of csMTR along the inner and middle surface may be partially redundant. However, it should be noted that the direct statistical tests performed in this study examined either (i) the difference between corresponding vertex points in MS patients and controls or (ii) the difference in csMTR between the inner and outer cortical boundaries. Since the same surface reconstruction was carried out for both patients and controls and the inner and outer cortical boundaries were generally well separated, we believe the vertex-based, statistical analysis we employed in this study was indeed robust.

Linking cortical MTR signal to underlying sub-pial myelin content also is subject to some confounds. Previous work has demonstrated that MTR on the cortical surface is an indicator of sub-pial demyelination in *ex-vivo* brain tissue (Chen et al., 2013). However, such MTR imaging of sub-pial myelin is still an indirect measure because it is weighted by the T_1 relaxation time, the homogeneity of B_1^+ excitation and off-resonance saturation pulses, and the MRI sequence parameters (Helms et al., 2008). Future research will investigate the use of magnetization transfer saturation (Helms et al., 2008) and bound pool fraction mapping (Davies et al., 2004) as alternatives to MTR for potentially more precise measurements of cortical myelin content.

In Table 3 we compared mean MTR in NACGM between patients and controls. No significant differences between patients and controls were found in this assessment, suggesting that sub-pial demyelination is not a completely global, whole-cerebrum effect. Instead, our data from Fig. 3 suggest it typically occurs in localized clusters in the vicinity of the primary motor strip, posterior cingulate gyrus, precuneus and cuneus, in addition to the inferior parietal and superior temporal lobes. Significant reductions in MTR were observed between lesion locations in patients compared to corresponding ROIs in controls, while controlling for spatial variations in csMTR. Although the application of a multi-contrast reading protocol, including DIR, allowed detection of many leukocortical lesions in our study, we recognize not all cortical lesions are faithfully detected using 3 T MRI. Therefore, the MTR values cited for cortical lesions in Table 3 correspond to those for a subset of cortical lesions.

The NAWM MTR (*i.e.* mean white matter MTR not including lesions) of patients in our study was significantly lower than that of controls,

suggesting patients in our study may have significant loss of myelin in cerebral white matter. The relationship between NAWM demyelination and cortical pathology remains an open area of research. In their comprehensive diffusion MRI and histopathology-based work, Kolasinski et al. (2012) demonstrated cell or axonal loss in a given white matter brain area may give rise to anterograde or retrograde degeneration in cortical areas distant from the site of initial white matter tissue damage. Further research is necessary to determine whether the well-recognized white matter inflammatory response observed in MS is linked to cortical pathology or whether these events occur independently of one another.

5. Conclusion

Multi surface-based MTR at the clinically accessible field strength of 3 T identifies cortical sub-pial abnormality suggestive of demyelination in MS patients. Our results suggest that parcellation of the brain using the Desikan-Killiany surface-based atlas allows identification of regional decreases in csMTR compared to controls. Using this information may allow better stratification of early changes in myelination of the cortex and more efficacious detection of treatment response.

Acknowledgements

We are especially grateful to all the study participants. The authors also wish to thank Ms. Rozie Arnaoutelis for her invaluable assistance in obtaining consents from and scheduling examinations for both patients and controls. D.A.R was supported in part by an endMS Postdoctoral Fellowship from the Multiple Sclerosis Society of Canada (MS Society of Canada Project/Grant #2296). Additionally, the authors wish to acknowledge funding from CIHR MOP# 84367 for this study.

References

Allman, J.M., Hakeem, A., Erwin, J.M., Nimchinsky, E., Hof, P., 2001. The anterior cingulate cortex. The evolution of an interface between emotion and cognition. Ann. N. Y. Acad. Sci. 935, 107–117.

Benjamini, Y., Yekutieli, D., 2001. The control of the false discovery rate in multiple testing under dependency. Ann. Stat. 1165–1188.

Bo, L., Vedeler, C.A., Nyland, H.I., Trapp, B.D., Mork, S.J., 2003. Subpial demyelination in the cerebral cortex of multiple sclerosis patients. J. Neuropathol. Exp. Neurol. 62, 723–732.

Bock, N.A., Hashim, E., Janik, R., Konyer, N.B., Weiss, M., Stanisz, G.J., Turner, R., Geyer, S., 2013. Optimizing T 1-weighted imaging of cortical myelin content at 3.0 T. NeuroImage 65, 1–12.

Campi, A., Filippi, M., Comi, G., Scotti, G., Gerevini, S., Dousset, V., 1996. Magnetisation transfer ratios of contrast-enhancing and nonenhancing lesions in multiple sclerosis. Neuroradiology 38, 115–119.

Chen, J.T., Easley, K., Schneider, C., Nakamura, K., Kidd, G.J., Chang, A., Staugaitis, S.M., Fox, R.J., Fisher, E., Arnold, D.L., Trapp, B.D., 2013. Clinically feasible MTR is sensitive to cortical demyelination in MS. Neurology 80, 246–252.

Cohen-Adad, J., Benner, T., Greve, D., Kinkel, R.P., Radding, A., Fischl, B., Rosen, B.R., Mainero, C., 2011. In vivo evidence of disseminated subpial T2* signal changes in multiple sclerosis at 7 T: a surface-based analysis. NeuroImage 57, 55–62.

Collins, D.L., Neelin, P., Peters, T.M., Evans, A.C., 1994. Automatic 3D intersubject registration of MR volumetric data in standardized Talairach space. J. Comput. Assist. Tomogr. 18, 192–205.

Crespy, L., Zaaraoui, W., Lemaire, M., Rico, A., Faivre, A., Reuter, F., Malikova, I., Confort-Gouny, S., Cozzone, P.J., Pelletier, J., Ranjeva, J.P., Audoin, B., 2011. Prevalence of grey matter pathology in early multiple sclerosis assessed by magnetization transfer ratio imaging. PLoS One 6, e24969.

Dale, A.M., Fischl, B., Sereno, M.I., 1999. Cortical surface-based analysis: I. Segmentation and surface reconstruction. NeuroImage 9, 179–194.

Davies, G.R., Tozer, D.J., Cercignani, M., Ramani, A., Dalton, C.M., Thompson, A.J., Barker, G.J., Tofts, P.S., Miller, D.H., 2004. Estimation of the macromolecular proton fraction and bound pool T2 in multiple sclerosis. Mult. Scler. 10, 607–613.

Derakhshan, M., Caramanos, Z., Narayanan, S., Arnold, D.L., Louis Collins, D., 2014. Surface-based analysis reveals regions of reduced cortical magnetization transfer ratio in patients with multiple sclerosis: a proposed method for imaging subpial demyelination. Hum. Brain Mapp. 35, 3402–3413.

Desikan, R.S., Segonne, F., Fischl, B., Quinn, B.T., Dickerson, B.C., Blacker, D., Buckner, R.L., Dale, A.M., Maguire, R.P., Hyman, B.T., Albert, M.S., Killiany, R.J., 2006. An automated labeling system for subdividing the human cerebral cortex on MRI scans into gyral based regions of interest. NeuroImage 31, 968–980.

Dousset, V., Grossman, R.I., Ramer, K.N., Schnall, M.D., Young, L.H., Gonzalez-Scarano, F., Lavi, E., Cohen, J.A., 1992. Experimental allergic encephalomyelitis and multiple sclerosis: lesion characterization with magnetization transfer imaging. Radiology 182, 483–491.

Filippi, M., Rocca, M.A., Martino, G., Horsfield, M.A., Comi, G., 1998. Magnetization transfer changes in the normal appearing white matter precede the appearance of enhancing lesions in patients with multiple sclerosis. Ann. Neurol. 43, 809–814.

Fischl, B., Sereno, M.I., Dale, A.M., 1999a. Cortical surface-based analysis: II: inflation, flattening, and a surface-based coordinate system. NeuroImage 9, 195–207.

Fischl, B., Sereno, M.I., Tootell, R.B.H., Dale, A.M., 1999b. High-resolution intersubject averaging and a coordinate system for the cortical surface. Hum. Brain Mapp. 8, 272–284.

Francis, S.J., 2005. Automatic Lesion Identification in MRI of Multiple Sclerosis Patients (2004). (Master's thesis). McGill University, Montreal, Quebec.

Geurts, J.J.G., Bö, L., Pouwels, P.J.W., Castelijns, J.A., Polman, C.H., Barkhof, F., 2005. Cortical lesions in multiple sclerosis: combined postmortem MR imaging and histopathology. Am. J. Neuroradiol. 26, 572–577.

Glasser, M.F., Van Essen, D.C., 2011. Mapping human cortical areas in vivo based on myelin content as revealed by T1-and T2-weighted MRI. J. Neurosci. 31, 11597–11616.

Glasser, M.F., Goyal, M.S., Preuss, T.M., Raichle, M.E., Van Essen, D.C., 2014. Trends and properties of human cerebral cortex: correlations with cortical myelin content. NeuroImage 93, 165–175.

Goldberg, R.F., Perfetti, C.A., Fiez, J.A., Schneider, W., 2007. Selective retrieval of abstract semantic knowledge in left prefrontal cortex. J. Neurosci. 27, 3790–3798.

Goldberg, R.F., Perfetti, C.A., Schneider, W., 2006. Perceptual knowledge retrieval activates sensory brain regions. J. Neurosci. 26, 4917–4921.

Helms, G., Dathe, H., Kallenberg, K., Dechent, P., 2008. High-resolution maps of magnetization transfer with inherent correction for RF inhomogeneity and T1 relaxation obtained from 3D FLASH MRI. Magn. Reson. Med. 60, 1396–1407.

Howell, O.W., Reeves, C.A., Nicholas, R., Carassiti, D., Radotra, B., Gentleman, S.M., Serafini, B., Aloisi, F., Roncaroli, F., Magliozzi, R., Reynolds, R., 2011. Meningeal inflammation is widespread and linked to cortical pathology in multiple sclerosis. Brain 134, 2755–2771.

Jenkinson, M., Beckmann, C.F., Behrens, T.E., Woolrich, M.W., Smith, S.M., 2012. FSL. NeuroImage 62, 782–790.

Kolasinski, J., Stagg, C.J., Chance, S.A., Deluca, G.C., Esiri, M.M., Chang, E.H., Palace, J.A., Mcnab, J.A., Jenkinson, M., Miller, K.L., Johansen-Berg, H., 2012. A combined post-mortem magnetic resonance imaging and quantitative histological study of multiple sclerosis pathology. Brain 135, 2938–2951.

Kurtzke, J.F., 1983. Rating neurologic impairment in multiple sclerosis an expanded disability status scale (EDSS). Neurology 33, 1444-1444.

Kutzelnigg, A., Lucchinetti, C.F., Stadelmann, C., Brück, W., Rauschka, H., Bergmann, M., Schmidbauer, M., Parisi, J.E., Lassmann, H., 2005. Cortical demyelination and diffuse white matter injury in multiple sclerosis. Brain 128, 2705–2712.

Leech, R., Sharp, D.J., 2014. The role of the posterior cingulate cortex in cognition and disease. Brain 137, 12–32.

Lerch, J.P., Evans, A.C., 2005. Cortical thickness analysis examined through power analysis and a population simulation. NeuroImage 24, 163–173.

Magliozzi, R., Howell, O., Vora, A., Serafini, B., Nicholas, R., Puopolo, M., Reynolds, R., Aloisi, F., 2007. Meningeal B-cell follicles in secondary progressive multiple sclerosis associate with early onset of disease and severe cortical pathology. Brain 130, 1089–1104.

Mainero, C., Benner, T., Radding, A., Van Der Kouwe, A., Jensen, R., Rosen, B.R., Kinkel, R.P., 2009. In vivo imaging of cortical pathology in multiple sclerosis using ultra-high field MRI. Neurology 73, 941–948.

Mainero, C., Louapre, C., Govindarajan, S.T., Gianni, C., Nielsen, A.S., Cohen-Adad, J., Sloane, J., Kinkel, R.P., 2015. A gradient in cortical pathology in multiple sclerosis by in vivo quantitative 7 T imaging. Brain 138, 932–945.

Margulies, D.S., Vincent, J.L., Kelly, C., Lohmann, G., Uddin, L.Q., Biswal, B.B., Villringer, A., Castellanos, F.X., Milham, M.P., Petrides, M., 2009. Precuneus shares intrinsic functional architecture in humans and monkeys. Proc. Natl. Acad. Sci. U. S. A. 106, 20069–20074.

Mascalchi, M., Toschi, N., Ginestroni, A., Giannelli, M., Nicolai, E., Aiello, M., Soricelli, A., Diciotti, S., 2014. Gender, age-related, and regional differences of the magnetization transfer ratio of the cortical and subcortical brain gray matter. J. Magn. Reson. Imaging 40, 360–366.

Mesaros, S., Rocca, M.A., Kacar, K., Kostic, J., Copetti, M., Stosic-Opincal, T., Preziosa, P., Sala, S., Riccitelli, G., Horsfield, M.A., Drulovic, J., Comi, G., Filippi, M., 2012. Diffusion tensor MRI tractography and cognitive impairment in multiple sclerosis. Neurology 78, 969–975.

Mistry, N., Abdel-Fahim, R., Mougin, O., Tench, C., Gowland, P., Evangelou, N., 2014. Cortical lesion load correlates with diffuse injury of multiple sclerosis normal appearing white matter. Mult. Scler. J. 20, 227–233.

Nelson, F., Datta, S., Garcia, N., Rozario, N.L., Perez, F., Cutter, G., Narayana, P.A., Wolinsky, J.S., 2011. Intracortical lesions by 3 T magnetic resonance imaging and correlation with cognitive impairment in multiple sclerosis. Mult. Scler. 17, 1122–1129.

Newbould, R.D., Nicholas, R., Thomas, C.L., Quest, R., Lee, J.S., Honeyfield, L., Colasanti, A., Malik, O., Mattoscio, M., Matthews, P.M., Sormani, M.P., Waldman, A.D., Muraro, P.A., 2014. Age independently affects myelin integrity as detected by magnetization transfer magnetic resonance imaging in multiple sclerosis. Neuroimage Clin. 4, 641–648.

Nielsen, A.S., Kinkel, R.P., Madigan, N., Tinelli, E., Benner, T., Mainero, C., 2013. Contribution of cortical lesion subtypes at 7 T MRI to physical and cognitive performance in MS. Neurology 81, 641–649.

Nielsen, A.S., Kinkel, R.P., Tinelli, E., Benner, T., Cohen-Adad, J., Mainero, C., 2012. Focal cortical lesion detection in multiple sclerosis: 3 Tesla DIR versus 7 Tesla FLASH-T2. J. Magn. Reson. Imaging 35, 537–542.

Papadopoulou, A., Muller-Lenke, N., Naegelin, Y., Kalt, G., Bendfeldt, K., Kuster, P., Stoecklin, M., Gass, A., Sprenger, T., Radue, E.W., Kappos, L., Penner, I.K., 2013.

Contribution of cortical and white matter lesions to cognitive impairment in multiple sclerosis. Mult. Scler. 19, 1290–1296.
Peterson, J.W., Bo, L., Mork, S., Chang, A., Trapp, B.D., 2001. Transected neurites, apoptotic neurons, and reduced inflammation in cortical multiple sclerosis lesions. Ann. Neurol. 50, 389–400.
Pike, G.B., de Stefano, N., Narayanan, S., Francis, G.S., Antel, J.P., Arnold, D.L., 1999. Combined magnetization transfer and proton spectroscopic imaging in the assessment of pathologic brain lesions in multiple sclerosis. Am. J. Neuroradiol. 20, 829–837.
Polman, C.H., Reingold, S.C., Edan, G., Filippi, M., Hartung, H.P., Kappos, L., Lublin, F.D., Metz, L.M., Mcfarland, H.F., O'connor, P.W., Sandberg-Wollheim, M., Thompson, A.J., Weinshenker, B.G., Wolinsky, J.S., 2005. Diagnostic criteria for multiple sclerosis: 2005 revisions to the "McDonald criteria". Ann. Neurol. 58, 840–846.
Rocca, M.A., Mastronardo, G., Rodegher, M., comi, G., Filippi, M., 1999. Long-term changes of magnetization transfer-derived measures from patients with relapsing-remitting and secondary progressive multiple sclerosis. AJNR Am. J. Neuroradiol. 20, 821–827.
Rocca, M.A., Pagani, E., Ghezzi, A., Falini, A., Zaffaroni, M., Colombo, B., Scotti, G., Comi, G., Filippi, M., 2003. Functional cortical changes in patients with multiple sclerosis and nonspecific findings on conventional magnetic resonance imaging scans of the brain. NeuroImage 19, 826–836.
Samson, R.S., Cardoso, M.J., Muhlert, N., Sethi, V., Wheeler-Kingshott, C.A., Ron, M., Ourselin, S., Miller, D.H., Chard, D.T., 2014. Investigation of outer cortical magnetisation transfer ratio abnormalities in multiple sclerosis clinical subgroups. Mult. Scler. 20, 1322–1330.
Schiavone, F., Charlton, R.A., Barrick, T.R., Morris, R.G., Markus, H.S., 2009. Imaging age-related cognitive decline: a comparison of diffusion tensor and magnetization transfer MRI. J. Magn. Reson. Imaging 29, 23–30.
Schmierer, K., Scaravilli, F., Altmann, D.R., Barker, G.J., Miller, D.H., 2004. Magnetization transfer ratio and myelin in postmortem multiple sclerosis brain. Ann. Neurol. 56, 407–415.
Silver, N.C., Barker, G.J., Macmanus, D.G., Tofts, P.S., Miller, D.H., 1997. Magnetisation transfer ratio of normal brain white matter: a normative database spanning four decades of life. J. Neurol. Neurosurg. Psychiatry 62, 223–228.
Tewarie, P., Schoonheim, M.M., Schouten, D.I., Polman, C.H., Balk, L.J., Uitdehaag, B.M., Geurts, J.J., Hillebrand, A., Barkhof, F., Stam, C.J., 2015. Functional brain networks: linking thalamic atrophy to clinical disability in multiple sclerosis, a multimodal fMRI and MEG study. Hum. Brain Mapp. 36, 603–618.
Tona, F., Petsas, N., Sbardella, E., Prosperini, L., Carmellini, M., Pozzilli, C., Pantano, P., 2014. Multiple sclerosis: altered thalamic resting-state functional connectivity and its effect on cognitive function. Radiology 271, 814–821.
Yekutieli, D., Benjamini, Y., 1999. Resampling-based false discovery rate controlling multiple test procedures for correlated test statistics. J. Stat. Plann. Inference 82, 171–196.
Yu, H.J., Christodoulou, C., Bhise, V., Greenblatt, D., Patel, Y., Serafin, D., Maletic-Savatic, M., Krupp, L.B., Wagshul, M.E., 2012. Multiple white matter tract abnormalities underlie cognitive impairment in RRMS. NeuroImage 59, 3713–3722.
Zackowski, K.M., Smith, S.A., Reich, D.S., Gordon-Lipkin, E., Chodkowski, B.A., Sambandan, D.R., Shteyman, M., Bastian, A.J., Van Zijl, P.C., Calabresi, P.A., 2009. Sensorimotor dysfunction in multiple sclerosis and column-specific magnetization transfer-imaging abnormalities in the spinal cord. Brain 132, 1200–1209.
Zhuang, Y., Zhou, F., Gong, H., 2015. Intrinsic functional plasticity of the sensorimotor network in relapsing-remitting multiple sclerosis: evidence from a centrality analysis. PLoS One 10, e0130524.